

Characterization of Hydroxyapatite Coating on 316L Stainless Steel by Sol–Gel Technique

Sarbjit Kaur^{a,*}, Niraj Bala^{b,**}, and Charu Khosla^{c,***}

^aIKGPTU Kapurthala, India

^bMechanical Engineering Department BBSBEC, Fatehgarh Sahib, India

^cCUJET, Chitkara University, Punjab, India

*e-mail: sarbjit.kaur@bbsbec.ac.in

**e-mail: niraj.bala@bbsbec.ac.in

***e-mail: charu.khosla@chitkara.edu.in

Received March 14, 2018; revised July 6, 2018; accepted July 6, 2018

Abstract—Biomaterials are used for developing implants and producing a part or facilitating a function of a human body in a safe, reliable, and economical manner. Sol–gel deposition is one of the best, simple and economical methods of surface modification. In the current work, hydroxyapatite $\text{Ca}_{10}(\text{PO}_4)_6(\text{OH})_2$, a bio-active material, has been prepared and then deposited on 316L stainless steel by the sol-gel coating method. The porosity percentage of hydroxyapatite coating was found to be 0.22. Electrochemical corrosion testing was carried out for both uncoated and sol-gel coated specimens. The coated specimens were characterized by the X-ray diffraction, scanning electron microscopy, energy dispersive X-ray spectroscopy, and cross-sectional analysis. The results revealed that the Ca/P ratio of the sol-gel coated steel was closer to that of a real human bone. It was found that hydroxyapatite-coated samples show better corrosion resistance and better implant properties as compared to those of the uncoated 316L stainless steel.

Keywords: biomaterials, bioactive, electrochemical, hydroxyapatite, sol-gel

DOI: 10.3103/S1068375519030104

1. INTRODUCTION

Biomaterials are used to heal or repair defective parts of a human body. Various materials including metals alloys, ceramics and polymers are used as the base material. Three classes of metals have been used for biomaterials, these include stainless steel alloys, Co–Cr alloys and Ti and its alloys. Among the metallic materials, 316L stainless steel (316LSS), with an extra-low carbon content, is most commonly used for orthopedic properties due to its low cost, good corrosion resistance, and better mechanical properties [1]. Some inorganic materials formed at elevated temperature are termed ceramics. They may be metallic or non-metallic in nature. Bio-ceramics are used to repair hard tissues or the skeleton. They may be bio-inert (alumina, zirconia), bio-resorbable (tri-calcium phosphate), or bioactive (hydroxyapatite (HAP)) coatings. The orthopedic implants are generally classified as temporary or permanent devices. Due to its relatively low cost and higher biocompatibility, 316LSS is commonly used for temporary devices [2]. These devices mostly include fixation to assist fracture healing. However, due to a high concentration of chloride inside the body, there is a high risk of galvanic and localized corrosion. Metal ions release may also be

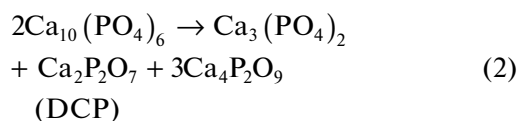
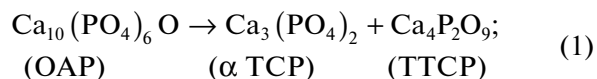
associated with such problems as cytotoxicity, genotoxicity, and carcinogenicity [3].

The surface of a bio-implant is modified by a coating with HAP, whose composition closely resemble the natural bone. It has good compatibility and is suitable for bone growth [2]. The main techniques used for coating biomaterials include thermal spray, sol gel, chemical vapour deposition, electrodeposition, biomimetic electrophoretic deposition, pulsed laser deposition, and ion beam sputtering [4–13]. Among thermal spray techniques, plasma spraying is mostly used for coatings. However, this technique has severe limitations such as a high working temperature which lowers the crystallinity of HAP and speed up the rate of dissolution of tri calcium phosphate (TCP), tetra calcium phosphate (TTCP), which leads to instability of an implant inside a human body [14]. Then a thicker coating also reduces corrosion resistance and exhibited porosity, which weakens the interfacial strength and leads to easy fractures [15]. A HAP coating on metallic alloys enhances the bone bonding ability, improves biocompatibility, and reduces the toxic effect of bio-implants on a living organism. In addition, the implanted material is expected to withstand applied physiological forces without substantial

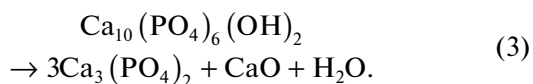
dimensional changes, catastrophic brittle fracture, or fracture in the long term creep, fatigue, or stress corrosion. In addition, these coatings lead to biocompatibility, provide a local source of calcium and phosphate ions required for bone cells to grow [16, 17]. In order to increase bioactivity, HAP coatings have been used. The combination of bioactive HAP coatings and mechanically strong metals has become a promising approach in fabrication of surgical implants for load-bearing applications. To modify the surface of the implant material, to generate new surface with different properties, bio ceramic coatings are commonly used. Sol-gel coating is the best method for prosthetic devices. It controls the coating morphology, chemistry, and structure [18–21]. A reduction in temperature is also possible according to the nature of additives/precursors chosen [22].

In medicine and dentistry, sol-gel coatings play an important role as they modify the surface area, porosity, composition, adsorption capacity, and dissolution rate. Most of the sol-gel coated materials are biodegradable. They can be used as fillers and sensors in different fields of biomaterials. Films can be produced by spin or dip deposition. Sol-gel coating method is used for uniform coating onto the surface of complex geometries of large dimension. This technique provides a protective [23–25] and bioactive [26, 27] coatings. It is a simple, low temperature coating technique through which pure, homogeneous films with thickness up to few micrometers [28] are formed. The substrates of 316LSS along with Ni-Ti and Ti alloys have been coated using this technique in order to improve their corrosion resistance [29–32]. Sol-gel coated HAP lowers the secretion of Ti and V ions from Ti alloys. This coating also improves osseointegration.

In a sol-gel route, when sintering at high temperature, i.e. at 1500°C, HAP gets decomposed to oxyhydroxyapatite (OHAP) or oxyapatite (OAP), which further dissociate to form TTCP, α TCP, dicalcium phosphate (DCP) and calcium oxide (CaO) at 1300°C, which is undesirable as illustrated by the following reactions and discussed in [33]:



or



Therefore, to avoid formation of these unwanted phases, in the present work, sol-gel coatings were formed at a lower temperature of 500°C to deposit HAP on 316LSS. Further, the as-coated specimens

were characterized by the X-ray diffraction (XRD), scanning electron microscopy (SEM), and energy dispersive spectroscopy (EDS). In vitro corrosion behavior of the uncoated 316LSS and of HAP coated specimens was investigated by the *Elog* extrapolation method in a Ringer's solution—a simulated body fluid.

2. EXPERIMENTAL

2.1. Sample Preparation

Specimens of 316LSS of 20 mm × 10 mm × 2 mm were prepared, polished with silicon carbide papers down to 180 grit. The specimens were blasted using grit blasting equipment. Al₂O₃ grits of 20 mesh sizes at a pressure of 5 bars for 2 minutes were used. The substrates were successively air blasted to remove any residual grit. The specimens were further washed with a mild detergent followed by water. Then the specimens were dipped into HNO₃ (20%) for 30 minutes to remove chemical impurity after grit blasting and to passivate them [34], after that rinsed with water, dried in air, and washed with acetone.

2.2. Sol-Gel Preparation

The sol-gel technique was selected with controlled dipping and withdrawal rates in order to vary the coating thickness. It involves Ca(NO₃)₂ and P₂O₅ as precursors of Ca and P, respectively, both biocompatible chemicals. The absolute alcohol was selected as the solvent. A simple dip coating apparatus was designed with adjustable rates of dipping. The method is simple, low-cost, easy in controlling the sintering temperature, and provides a homogeneous smooth coating. The process is shown in Fig. 1. Via this process, common implants such as mandibular, pedicle, and hip prosthesis can be coated smoothly.

The ceramic sol gel was prepared by using 2M Ca(NO₃)₂ in 50 mL ethanol and 3.1M P₂O₅ in 50 mL ethanol. An equal amount of Ca(NO₃)₂ and P₂O₅ were mixed to obtain Ca/P molar ratio of 1.67. Both solutions were mixed thoroughly with constant stirring, followed by refluxing for 24 hours. The resulting solution was taken in a round bottom conical flask; a condenser was connected in order to distill the solution taken in flask and water was circulated by connecting one end of the condenser to the tap and the other one to the sink. A temperature knob was adjusted accordingly so that solution may not boil. P₂O₅ reacts with alcohol to form oxyalkoxide with liberation of water. The latter was used for partial hydrolysis of oxyalkoxide and phosphorus precursors, which leads to the formation of gel.

2.3. Deposition of Coatings

The deposition was carried out by a simple belt-and-pulley type apparatus in order to dip the speci-

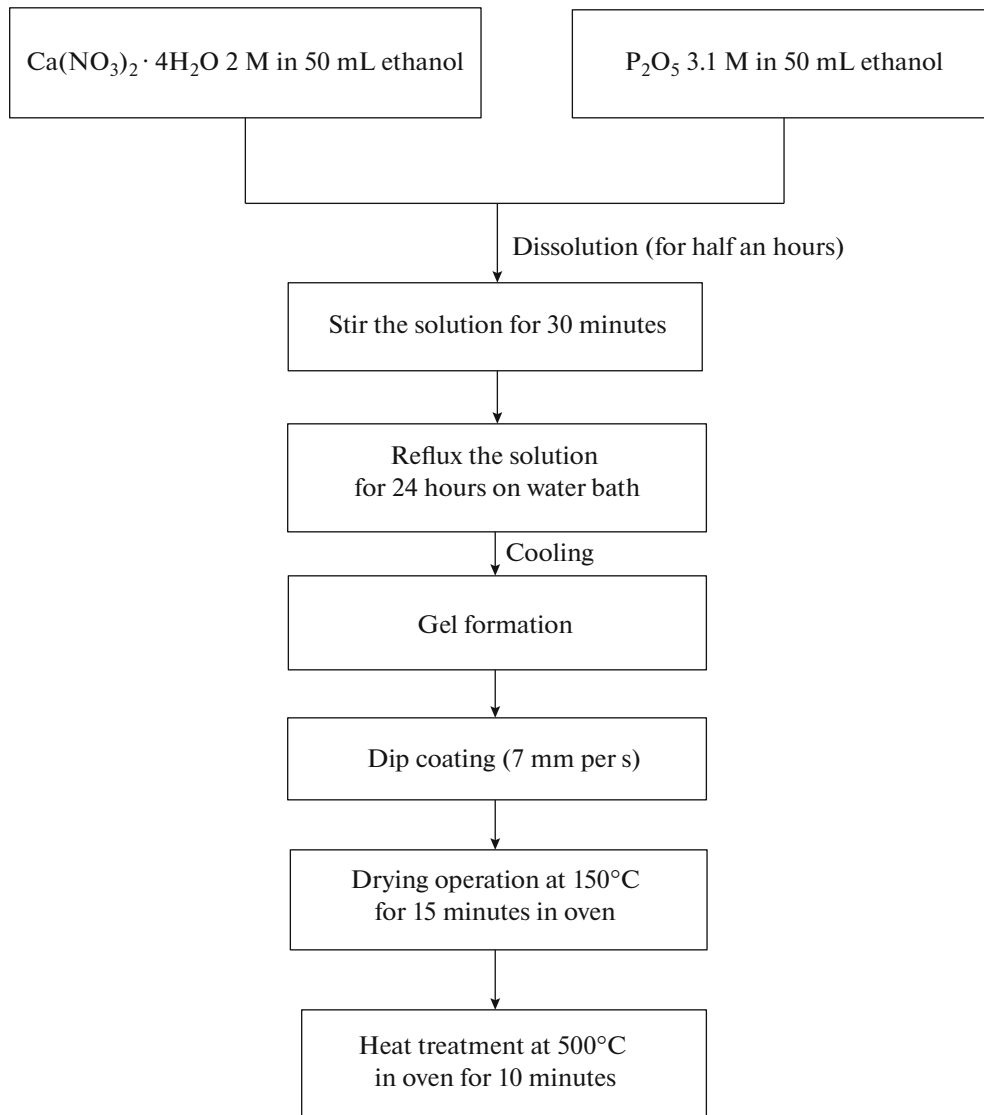


Fig. 1. Flow chart of sol-gel coating procedure.

mens into the gel. The apparatus has a switch to ascend and descend the substrate in and out of the gel for dip coating. The specimens were coated with ceramic thin films. The process was repeated at a constant dipping rate of 7 mm/s. The coating thickness was controlled by varying the dipping time. After dipping, the specimens were dried in an oven at 120°C for 24 hours in a silica crucible. This was followed by sintering in which the as-coated specimens were placed in an oven at 150°C for 15 minutes and then in a muffle furnace at 500°C for 10 minutes. After that, the specimens were placed in a desiccator having granular silica gel (to adsorb moisture) in order to attain the room temperature slowly. Next, the dipping was repeated followed by sintering at 150 and 500°C. The whole cycle was repeated 5 times in order to obtain the required thickness.

2.4. Characterization of Coatings

An XRD machine (X'pert-PRO) using Cu as anode, K_{α} radiation, operating at 45KV/40 mA, was used to determine the as-coated samples over the 2θ range of 20°–60°. To study the morphology of as-coated specimens, both XRD and SEM were performed; the compositions of various coatings were determined by EDS analysis.

X-ray mapping was carried out using a cross-sectional analysis. A low-speed precision saw was used for sectioning of all as-coated specimens, then a hot mounting press was used to mount the specimens. The mounted specimens were polished with emery paper of 200, 400, 600, 800, 1000, 1500, and 2000 grades, and finally slurry of alumina was used for mirror polishing. The cross-sectional morphology was analyzed by

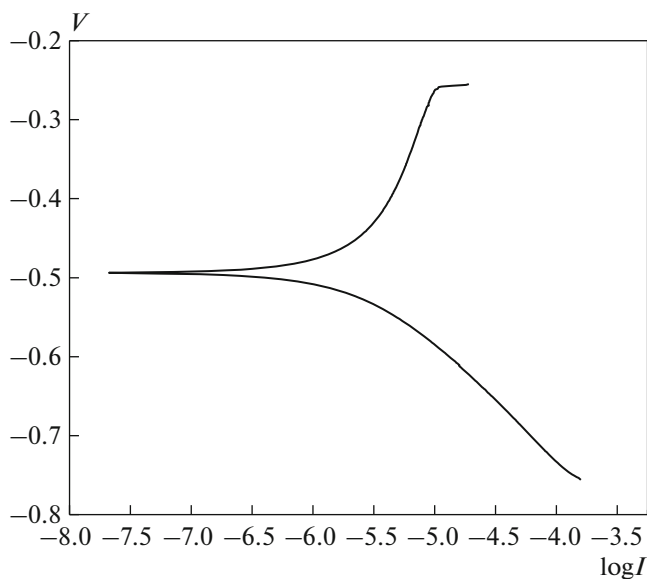


Fig. 2. Potentiodynamic curves of sol-gel coated SS HAP on 316LSS specimen in Ringer solution.

SEM and the distribution of various elements in as-coated samples was carried out by EDS analysis.

2.5. Porosity

Porosity of sol-gel coatings was estimated by an Inverted Optical microscope, connected with a computer fitted with an image-analyzing software (Zeiss Axiovision, Release 4.1). The images of the coatings were captured with an optical microscope and depicted with help of an imaging software. A minimum of 15 pictures were taken at different selected areas. The percentage porosity was evaluated by the difference in color of the pores and the bulk coating, with the help of an imaging software.

2.6. Coating Thickness Measurement

The thickness of the coating was determined by the cross-sectional analysis. An average of the coating thickness was carried out using a SEM micrograph and it was found to be 250 μm approximately.

Table 1. Parameters of sol-gel coated and uncoated 316LSS in Ringer solution at $37 \pm 1^\circ\text{C}$ temperature

Parameters	Uncoated 316LSS	HAP coated 316 LSS
E_{corr} , mV	-365	-493.8
$I_{\text{corr}}e^{-6}$, A cm^{-2}	1.696	1.61
CRe^{-3} , mpy	764.9	640

2.7. Electrochemical Corrosion

A potentiostat/galvanostat (Series G-750), interfaced with a computer and loaded with Gamry electrochemical software DC105 was used. Electrochemical behavior of the bare and that of the sol-gel coated 316LSS was carried out using potentiodynamic polarization test with Ringer's solution, a simulated body fluid (SBF), at pH 7.2. The chemical composition (g/L) of Ringer's solution was: NaCl = 9 g, CaCl_2 = 0.24 g, KCl = 0.43 g, NaHCO_3 = 0.25 g.

Each specimen was dipped in the SBF solution for 24 hours at a temperature of $37 \pm 1^\circ\text{C}$ (as normal human body temperature), using heating mantle, to check the behavior of implants inside the body. For each specimen, 1 cm^2 area was exposed to the SBF solution; the saturated calomel electrode was used as reference electrode and the counter electrode was a graphite rod. The specimen performed the function of a working electrode. A fresh Ringer's solution was used for each specimen, the scan rate being 1 mv/s. The corrosion rate was determined using the Elog plots sweeping potential from -250 to $+250$ mV relative to the open circuit potential. To check the variation in microstructure and composition, SEM/EDS was carried out before and after immersion.

3. RESULTS

3.1. In vitro Corrosion Behavior

3.1.1. Electrochemical corrosion testing. The electrochemical corrosion behavior of the bare and of the as-sprayed coated specimens was studied using the procedure discussed in Section 2.7. The potentiodynamic curves of both as-coated and bare 316LSS specimens in Ringer's solution at $37 \pm 1^\circ\text{C}$ were obtained and shown in Figs. 2 and 3, respectively. The parameters of both coated and uncoated samples in Ringer's are given in Table 1.

It illustrates a high corrosion current density ($I_{\text{corr}} = 1.696e^{-6} \text{ A cm}^{-2}$, $E_{\text{corr}} = -365$ mV) and the corrosion rate ($\text{CR} = 764.9e^{-3}$ mpy) of uncoated 316LSS. The sol-gel coated specimen showed a corrosion current density ($I_{\text{corr}} = 1.61e^{-6} \text{ A cm}^{-2}$, $E_{\text{corr}} = -493$ mV) and corrosion rate ($\text{CR} = 640e^{-3}$ mpy), which are lower than those of a bare specimen. The higher the value of the corrosion current density (I_{corr}) at a given potential, the higher is the corrosion rate. The sol-gel coated specimens were successful in reducing corrosion.

3.2. X-Ray Diffraction

3.2.1. X-ray diffraction of as-coated samples. An XRD analysis of sol-gel coated samples is illustrated in Fig. 4. The ICDD card no. 01-073-1731 confirmed the presence of HAP ($\text{Ca}_{10}(\text{PO}_4)_6(\text{OH})_2$) and the card no. 00-009-0077 proved the presence of calcium phosphate hydroxide hydrate ($\text{CaPO}_3(\text{OH})_2\text{H}_2\text{O}$) (α)

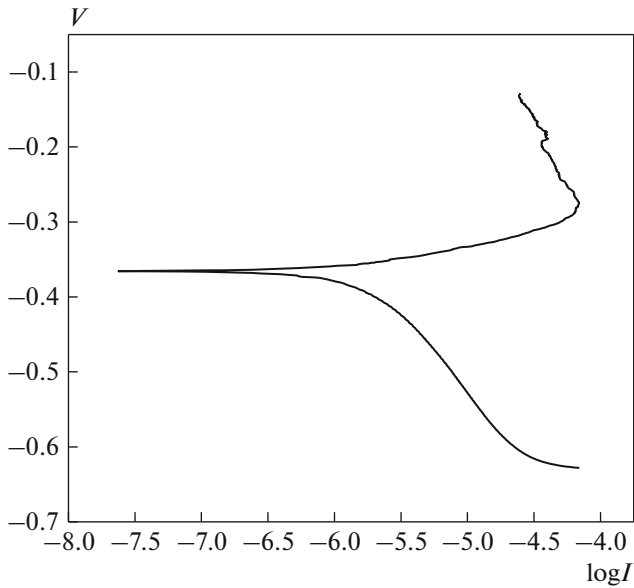


Fig. 3. Potentiodynamic curves of uncoated 316L specimen in Ringer solution.

and calcium hydrogen phosphate hydrate ($\text{Ca}_8(\text{HPO}_4)_2(\text{PO}_4)_4(\text{H}_2\text{O})_5$ (β). These additional products were formed due to heating the as-coated samples at 500°C repeatedly. Still, the working temperature of deposition was lower than the melting point of HAP (1050°C), so HAP did not decompose to form TCP and TTCP, which are undesirable for longevity of bio implants.

3.2.2. XRD of as-coated samples after immersion in SBF. XRD peaks of sol-gel coated HAP after electrochemical corrosion testing are shown in Fig. 5. The sharpness of peaks improved after immersion in SBF for 24 hours and the coatings appeared to be more crystalline. Better crystallinity leads to a longer implant life. The presence of sharp peaks depicts the dissolution of amorphous phase during immersion. The broadening of peaks and low intensity of peaks symbolizes the presence of an amorphous phase [35]. The ICDD card no. 01-073-1731 confirmed the presence of HAP (h) even after immersion and peaks appeared to be sharper, and the card no. 01-079-0423 confirmed the presence of calcium hydrogen phosphate hydrate (β). The presence of calcium hydrogen phosphite hydrate (α) was proved by the card no. 00-046-0494.

The peaks of calcium phosphate hydroxide hydrate, which were observed in as-coated specimens, disappeared after corrosion; they might have dissolved after immersion. An XRD analysis predicted that the bare specimen was uniformly covered with a layer of iron oxide (Fig. 6). The Fe_2O_3 phase with the ICDD card no. 01-076-1470 has been depicted along with minor peaks of iron oxide phosphate with the ICDD card no. 00-050-1634.

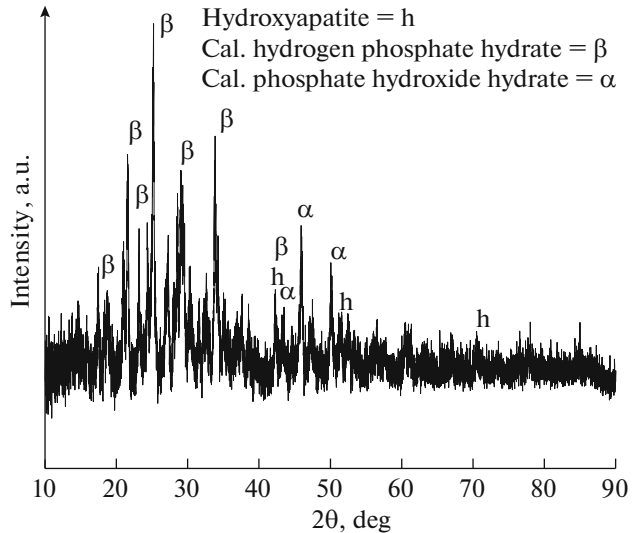


Fig. 4. X-ray diffraction pattern of sol-gel coated HAP on 316LSS, [HAP (h), Calcium phosphate hydroxide hydrate (α) and calcium hydrogen phosphate hydrate (β)].

3.3. SEM/EDS Analysis

3.3.1. SEM/EDS surface analysis of as-coated samples. The oxide layers formed on the surface of the substrates of biomaterials are of prime importance, as these layers come in a direct contact with the tissues of living organisms [36]. The long term biological interaction and the corrosion behavior of an implant are determined by the specific properties of the oxide film such as defect density, stoichiometry, crystal structure, and surface topography [37]. The destruction of the implant metal during its exposure to the human

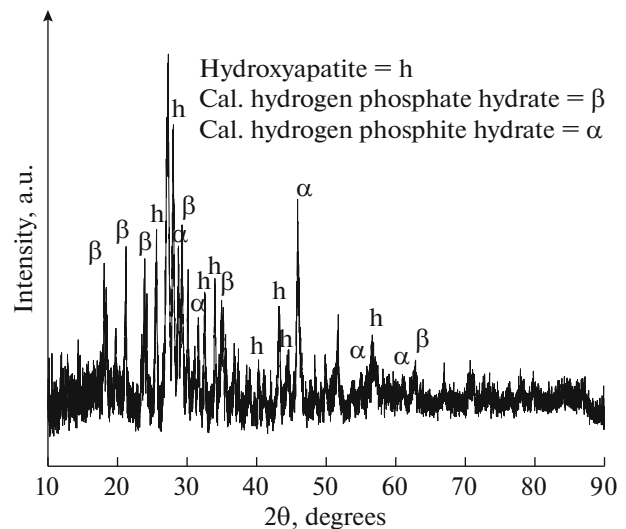


Fig. 5. X-ray diffraction pattern of sol-gel coated HAP on 316LSS, after immersion in Ringer solution [HAP (h), Calcium hydrogen phosphite hydrate (α) and calcium hydrogen phosphate hydrate (β)].

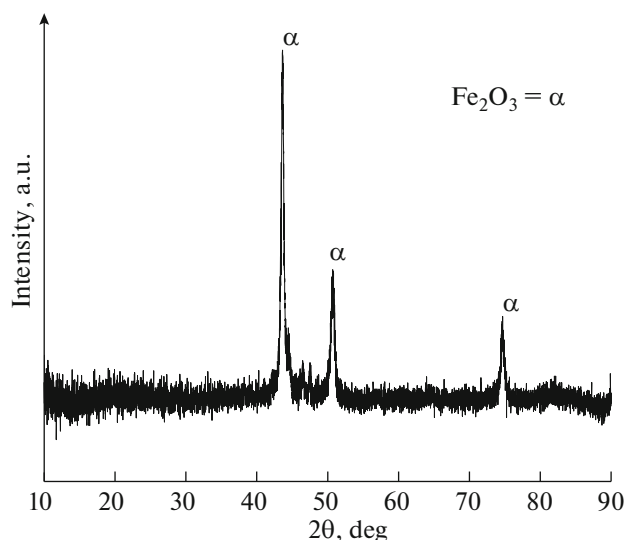


Fig. 6. X-ray diffraction pattern of uncoated 316LSS, after immersion in Ringer solution.

body environment highly depends upon the stability of the protective oxide layer. The specimens were further examined by SEM/EDS for the microstructural analysis of their surfaces and to detect the compositional changes, if any.

The SEM morphology of HAP coatings on 316LSS by sol-gel route is shown in Fig. 7. A dense and thick crystalline HAP coating has been obtained after heat treatment at 150°C for 5 min and at 500°C for 15 minutes. The EDS analysis of a HAP coated sample (Fig. 8) depicts the presence of main elements such as calcium (Ca), phosphorous (P), and oxygen (O). The Ca/P ratio comes out to be 1.44, as shown in Table 2, which is close to that of a real actual bone, i.e. 1.67. A slight deviation indicates the presence of other compounds like calcium hydrogen phosphate hydrates and calcium phosphate hydroxide hydrate. The coating remains intact and crack free due to a low sintering temperature.

3.3.2. SEM/EDS of as-coated samples after immersion in SBF. The microstructure of the corroded specimens after immersion in Ringer's solution has been analyzed by SEM/EDS. To the best of the authors' knowledge, there are only a few studies which

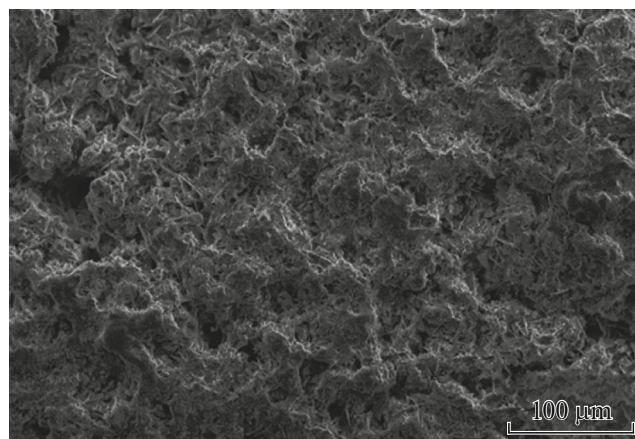


Fig. 7. SEM analysis of sol-gel coated HAP on 316LSS.

report the microstructure of sol-gel HAP coatings after their corrosion testing in SBF solution.

A SEM micrograph (Fig. 9) shows the retained morphology even after immersion, which is a positive attribute. The SEM/EDS micrographs of as-coated HAP after immersion in SBF solution for 24 hours are depicted in Fig. 10. Calcium and phosphorous were determined to be the main components in the coatings (Fig. 10). The Ca/P ratio of as-coated specimens before and after dipping has been determined by the EDS analysis, as shown in Table 2. The variations in the Ca/P ratio demonstrate the presence of different calcium phosphate compounds in coatings. The as-coated specimens after immersion showed reduction in the Ca/P ratio, which is due to the presence of O and to the corrosion of the base metal, to some extent, in SBF. A higher percentage of O and C in HAP coatings on both substrates indicates a probable formation of oxides and carbides. As clear from Fig. 10, the coating seems to be porous and crack free. Some phases may undergo dissolution in SBF, which lowers the Ca/P ratio to 1.128, while before immersion it was 1.44 as shown in Table 2. Due to the presence of various salts in SBF, the HAP undergoes oxidation and the calcium phosphate hydroxide hydrate ($\text{CaPO}_3(\text{OH})_2\text{H}_2\text{O}$) phase disappears in SBF solution, then calcium hydrogen phosphite hydrate is formed, the latter also has been confirmed by XRD.

3.4. Cross-Sectional Analysis

3.4.1. Cross-sectional analysis of as-coated specimens. The cross-sectional SEM/EDS analysis was performed for the sol-gel coated sample. The coating thickness measured from the micrograph was 250 μm approximately. Figure 11 showed the X-ray mapping analysis of HAP coated 316LSS specimen, with Fe, Cr and Ni being detected in base metals. The mapping of Ca and P elements clearly indicated that these elements co-exist and are uniformly distributed; O was

Table 2. Ca/P ratio of sol-gel coated 316LSS before and after corrosion testing

S. No.	Type of coating	Before/After corrosion testing	Ca/P
1	Pure HAP coating	Before	1.44
2	Pure HAP coating	After	1.128

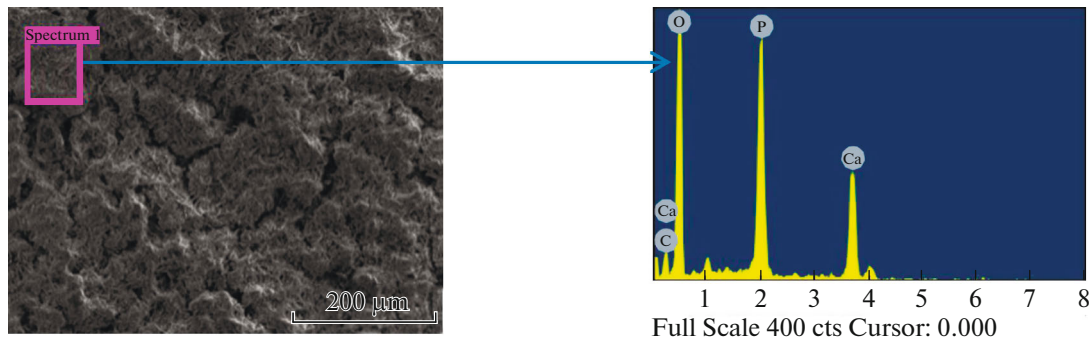


Fig. 8. SEM/EDS point analysis showing the elemental composition of sol-gel coated HAP on 316LSS.

present throughout the coating. There was no diffusion of elements between the coating and the base metal.

3.4.2. Cross-sectional analysis of as-coated specimens after immersion in SBF. A cross-sectional elemental analysis of sol-gel coated specimens after immersion in Ringer's solution are shown in Fig. 12. That Fig. 12 indicates that the coating successfully retained its micro-structure even after electrochemical corrosion testing. Cr, Ni, and Fe elements were detected in the substrate in both bare and as-coated specimens, before and after corrosion testing. Ca and P were the main components detected whereas O was present throughout. The elemental analysis depicts that sol-gel coating was successful to prevent the diffusion of various elements in the alloy. As shown in Fig. 12, the Ca and P components dissolved to a small extent in SBF and the content of oxygen increased. This has been verified by the SEM/EDS analysis and the reduction of the Ca/P ratio has also been observed.

3.5. Porosity

The values of porosity of the sol-gel coated specimen was found to be 0.22. The HAP coated specimen shows lower porosity as a dense coating act as barrier to dissolution of the material and also provides better corrosion resistance. As the porosity affects the mechanical properties of the implant, a lower percentage porosity helps bone growth and its fixation, whereas a higher percentage porosity leads to fractures and also affects certain mechanical properties [38].

4. DISCUSSION

Sol-gel route is a simple and economical technique to deposit HAP in comparison to other thermal spray methods. This technique results in a high quality thin HAP layer deposition on steel, which imparts compact biological affinity to the substrate for medical applications. HAP has been successfully deposited on 316LSS by sol-gel method. The HAP powder formation required 350°C, while a temperature of 375°C and

400°C was required to deposit apatite phase for coatings on the roughened 316LSS [39].

Potentiodynamic polarization study revealed that sol-gel coated specimens reduced corrosion as determined after dipping in SBF for 24 hours at $37 \pm 1^\circ\text{C}$, and it confirmed that the dense corrosion resistance coatings are in agreement with others in [40] and [41], the latter depositing HAP coating on Ti-6Al-4V using sol-gel technique. The authors in [42] also applied the sol gel method as well as electrophoresis to deposit HAP on Ti sheets and found that homogeneous coatings were obtained; and a sol-gel coating showed superior crystallinity over an electrophoresis coating. The coated samples showed high corrosion resistance in agreement with [41].

XRD as well as SEM have shown that a homogeneous coating can be formed, which is in agreement with [43]. The XRD analysis indicated that the peaks corresponding to HAP become more prominent near $31^\circ\text{--}32^\circ \theta$ after immersion in SBF; the ICDD card no. 01-073-1731 confirmed the presence of HAP ($\text{Ca}_{10}(\text{PO}_4)_6(\text{OH})_2$). The peaks become more prominent after immersion due to dissolution of the amorphous phases in SBF and in the coating, as well as

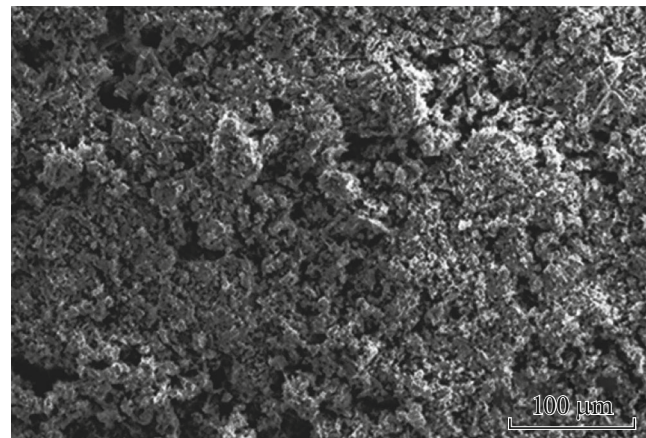


Fig. 9. SEM analysis of sol-gel coated HAP on 316LSS after immersion in Ringer solution.

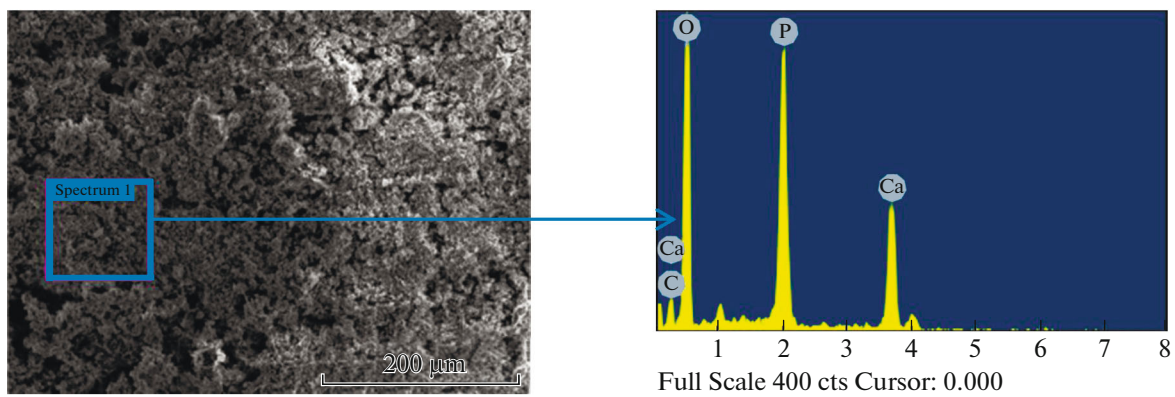


Fig. 10. SEM/EDS point analysis showing the elemental composition of sol-gel coated HAP on 316L SS after immersion in Ringer solution.

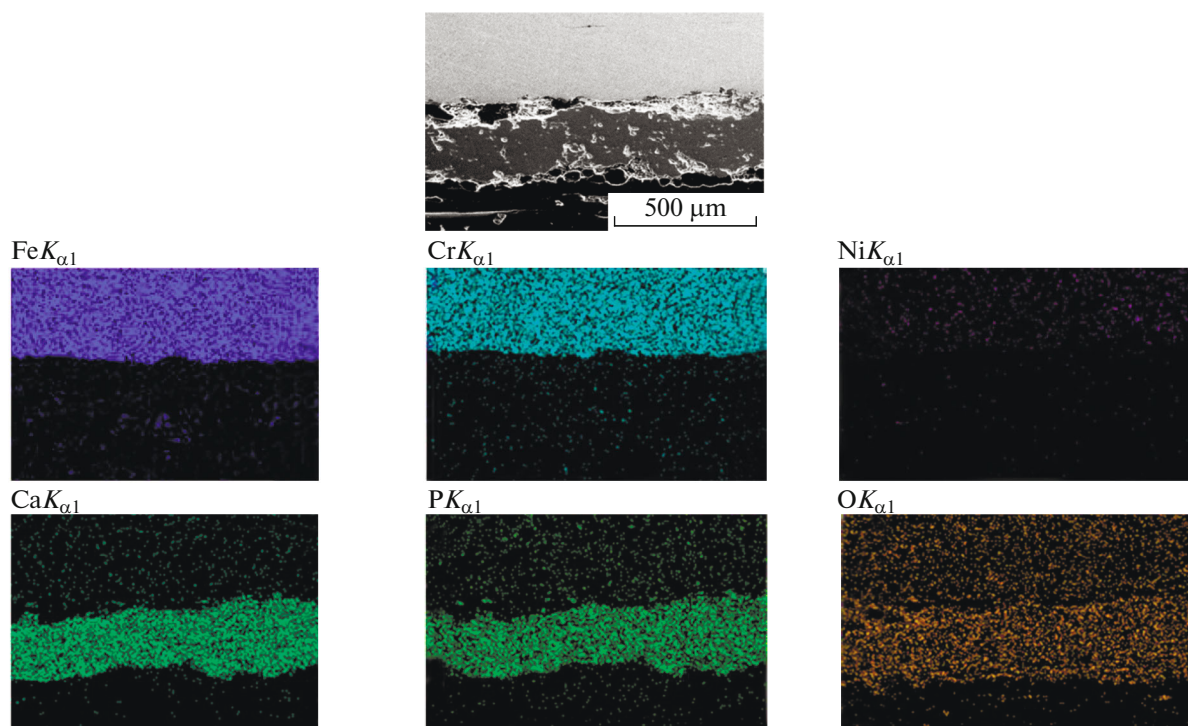


Fig. 11. Cross-sectional EDS elemental maps of sol-gel coated HAP on 316LSS.

more crystalline phases. As reported elsewhere, sintering at 750°C can lead to the formation of cracks [44]. To overcome this problem, they added either P_2O_5 or glycerol to the sol. Further repetition of dipping also reduced the cracks. In order to avoid the formation of cracks, in the present study, a simple method based on refluxing of the calcium and phosphorous precursors was adopted to accomplish pure HAP deposition at 500°C, since other methods involved very high temperature as reported elsewhere [33].

The *in vitro* corrosion behavior of Ti, Ti–6Al–6Nb and Ti–6Al–4V implant materials coated with sol-gel

derived HAP has been investigated by others [45], who found that crystalline HAP and β -TCP coatings on the implants revealed beneficial corrosion protection effect during prolonged exposure to the Hank's balanced salt solution.

SEM/EDS micrographs obtained turned to be quite similar to those in [40], whose authors followed the same route and deposited HAP on Ti–6Al–4V at 500°C. The Ca/P ratio also comes to closer to 1.6 that of a real bone, for the as-coated specimens as well as after immersion in SBF for 24 hours at a normal body temperature.

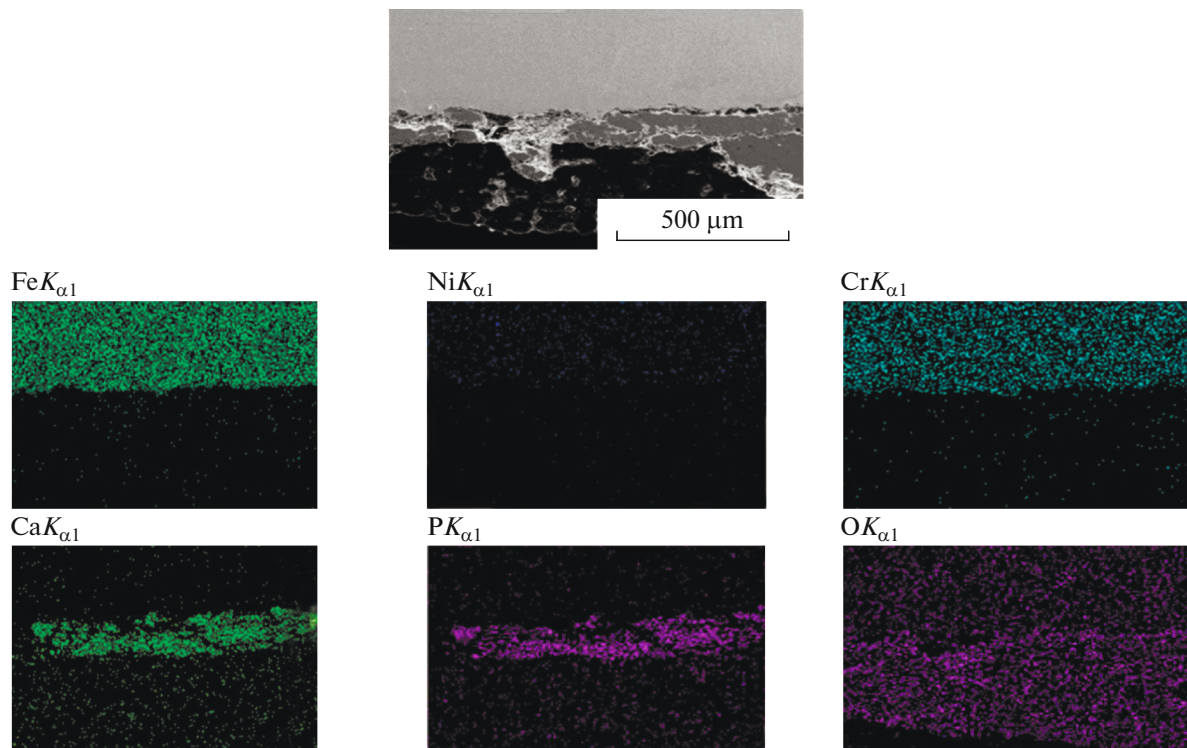


Fig. 12. Cross-sectional EDS elemental maps of sol-gel coated HAP on 316LSS after immersion in Ringer solution.

The SEM micrograph indicates the presence of micro pores in the coating; it is pertinent to mention that these micro pores may enhance the spreading, adhesion, and proliferation of osteoblasts [46]. A comparison of the EDS analysis of both HAP coated specimens before and after corrosion testing shows that the atomic percentage of Ca and P has decreased, whereas that of O increased after their immersion in Ringer's solution. The supremacy of O and C in the elemental composition indicates the formation of various oxides and carbides in the coatings.

As clear from XRD and SEM/EDS, the HAP coating remained intact even after immersion in SBF. A cross-sectional analysis also clearly indicated that deposition remains successful even after immersion in SBF for 24 hours and there was no diffusion of components among the coating and the substrate.

CONCLUSIONS

In the present study, we have prepared sol-gel derived HAP and its coating on 316LSS implants, in vitro, for orthopedic applications.

The obtained results showed that the prepared coatings were crystalline.

XRD confirmed the deposition of HAP, which was further confirmed by the SEM/EDS analysis.

Potentiodynamic polarization study revealed that sol-gel coated specimens reduced the corrosion rate after dipping in SBF (Ringer solution) for 24 hours.

No cracks were formed on the surface even after immersion in SBF as depicted by the SEM analysis.

ACKNOWLEDGMENTS

Authors express their earnest thanks to Dr. Harpreet Singh, Professor at the School of Mechanical, Materials and Energy Engineering, Indian Institute of Technology, Roopnagar (Punjab) and Metallizing equipment Industry, Jodhpur for their kind co-operation during this research work. Authors would also like to thank IKGPTU Kapurthala for providing access to papers and journals required for this research.

CONFLICT OF INTEREST

The authors declare that they have no conflict of interest.

REFERENCES

1. Manivasagam, G., Dhinasekaran, D., and Rajamanickam, A., *Corros. Sci.*, 2010, vol. 2, pp. 40–54.
2. Geesink, R.G., Groot, K., and Klein, C.P., *Clin. Orthop. Relat. Res.*, 1987, vol. 225, pp. 147–170.
3. Singh, R. and Dahotre, N.B., *J. Mater. Sci. Mater. Med.*, 2007, vol. 18, no. 5, pp. 725–751.

4. Chen, J.-Z., Shi, Y.-L., Wang, L., Yan, F.-Y., and Zhang, F.-Q., *Mater. Lett.*, 2006, vol. 60, no. 20, pp. 2538–2543.
5. Lee, J.-H., Kim, H.-E., and Koh, Y.-H., *Mater. Lett.*, 2009, vol. 63, pp. 1995–1998.
6. Lauenburg, S.C.G., Wolke, J.G.C., Siebers, M.C., Schoonam, J., et al., *Biomaterials*, 2006, vol. 27, pp. 3368–3378.
7. Milell, E., Cosentino, F., Licciuli, A., and Massaro, C., *Biomaterials*, 2001, vol. 22, pp. 1425–1431.
8. Sridhar, T.M., Mudali, U.K. and Subbaiyan, M., *Corros. Sci.*, 2003, vol. 45, pp. 237–252.
9. Wang, C.X., Chen, Z.Q., Guan, L.M., Wang, M., et al., *Nucl. Instrum. Methods Phys. Res., Sect. B*, 2001, vol. 179, pp. 364–372.
10. Nelea, V., Morosanu, C., Lliescuc, M., and Mihailescu, I.N., *Surf. Coat. Technol.*, 2003, vol. 173, pp. 315–322.
11. Khandewala, H., Singh, G., Aggarwal, K., Parkash, S., et al., *Appl. Surf. Sci.*, 2013, vol. 265, pp. 30–35.
12. Bala, N., Singh, H., Karthikeyan, J., and Parkash, S., *Surf. Eng.*, 2014, vol. 30, no. 6, pp. 414–421.
13. Singh, G., Singh, H., and Sidhu, B.S., in *Proc. Int. Thermal Spray Conf., May 10–12, Shanghai, China*, Materials Park, OH: ASM Int., 2016, pp. 812–819.
14. Sergo, V., Sbaizero, O., and Clarke, D.R., *Biomaterials*, 1997, vol. 18, no. 6, pp. 477–482.
15. Ahn, S.A., Choi, Y.S., Kim, J.G., and Han, J.G., *Surf. Coat. Technol.*, 2002, vol. 150, nos. 2–3, pp. 319–326.
16. Manso, M., Jiménez, C., Morant, C., Herrero, P., et al., *Biomaterials*, 2000, vol. 2, pp. 1755–1761.
17. Haddow, D.B., Kothari, S., James, P.F., and Short, R.D., *Biomaterials*, 1996, vol. 17, pp. 501–507.
18. Yildirim, O.S., Aksakal, B., Hanyaloglu, S.C., Erdogant, F., and Okur, A., *Spine (Philadelphia)*, 2006, vol. 31, no. 8, pp. E215–E220.
19. Turniansky, A., Avnir, D., Bronstein, A., et al., *J. Sol-Gel Sci. Technol.*, 1997, vol. 7, no. 1, pp. 135–143.
20. Brinker, C.J., Raman, N.K., Logan, M.N., et al., *J. Sol-Gel Sci. Technol.*, 1995, vol. 4, pp. 117–133.
21. Yildirim, O.S., Aksakal, B., Celik, H., Vangolu, Y., and Okur, A., *J. Med. Eng. Phys.*, 2005, vol. 27, no. 3, pp. 221–228.
22. Zarzycki, J., *J. Sol-Gel Sci. Technol.*, 1997, vol. 8, nos. 1–3, pp. 17–22.
23. de Sanctis, O., Gómez, L.G., Pellegrini, N., et al., *J. Non-Cryst. Solids*, 1990, vol. 121, pp. 338–343.
24. de Damborenea, J.J., Pellegrini, N., de Sanctis, O., and Durán, A., *J. Sol-Gel Sci. Technol.*, 1995, vol. 4, pp. 239–244.
25. Galliano, P., de Damborenea, J.J., Pascual, M.J., and Durán, A., *J. Sol-Gel Sci. Technol.*, 1998, vol. 13, pp. 723–727.
26. Gallardo, J. and Galliano, P., *J. Sol-Gel Sci. Technol.*, 2001, vol. 21, pp. 65–74.
27. Gallardo, J., Moreno, R., Galliano, P. and Durán, A., *J. Sol-Gel Sci. Technol.*, 2000, vol. 19, pp. 107–111.
28. Kokubo, T., *J. Non-Cryst. Solids*, 1990, vol. 120, pp. 138–151.
29. Black, J., *Biological Performance of Materials: Fundamentals of Biocompatibility*, New York: Marcel Dekker, 1992, 2nd ed.
30. Pereira, M., Clark, A., and Hench, L., *J. Am. Ceram. Soc.*, 1995, vol. 78, pp. 2463–2468.
31. Pereira, M. and Hench, L., *J. Sol-Gel Sci. Technol.*, 1996, vol. 7, pp. 59–68.
32. Cho, S., Miyagi, F., Kokubo, T., Nakanishi, K., et al., *J. Ceram. Soc. Jpn.*, 1996, vol. 104, pp. 399–404.
33. Liao, C.-J., Lin, F.-H., Chen, K.-S., and Sun, J.-S., *Biomaterials*, 1999, vol. 20, pp. 1807–1813.
34. Aksakal, B. and Hanyaloglu, C., *J. Mater. Sci. Mater. Med.*, 2008, vol. 19, pp. 2097–2104.
35. Singh, G., Singh, H., and Sidhu, B.S., *J. Biomimetics, Biomater., Tissue Eng.*, 2013, vol. 18, no. 1, p. 103. <https://doi.org/10.4172/1662-100X.1000103>
36. Nicholson, J.W., *The Chemistry of Medical and Dental Materials*, Cambridge: Royal Society of Chemistry, 2002.
37. Metikos-Huković, M., Kwoka, A., and Piljac, J., *Biomaterials*, 2003, vol. 24, no. 21, pp. 3765–3775.
38. Schwartz, Z. and Boyan, B.D., *J. Cell Biochem.*, 1994, vol. 56, no. 3, pp. 340–347.
39. Liu, D.M., Troczynski, T., and Tseng, W.J., *Biomaterials*, 2001, vol. 21, pp. 1721–1730.
40. Anjaneyulu, U., Priyadarshini, B., Arul Xavier Stango, S., Chellappa, M., Geetha, M., and Vijayalakshmi, U., *Mater. Technol.: Adv. Perform. Mater.*, 2010, vol. 20, pp. 1753–1761.
41. El Hadad Amir, A., Peón Avés, E., García-Galván, F.R., Barranco, V., et al., *Materials (Basel)*, 2017, vol. 10, no. 2, p. 94. <https://doi.org/10.3390/ma10020094> PMID: PMC5459123
42. Peón Avés, E., Soares Sader, M., Rodrigues Jerônimo, F.A., de Sena, L.Á., et al., *Materia (Rio de Janeiro)*, 2007, vol. 12, no. 1. <https://doi.org/10.1590/S1517-70762007000100020>
43. Aksakal, B. and Hanyaloglu, C., *J. Mater. Sci. Mater. Med.*, 2008, vol. 19, pp. 2097–2104. <https://doi.org/10.1007/s10856-007-3304-in C>
44. Wei M., Ruys J., Milthorpe K., Sorrell C.C., and Evans J.H., *J. Sol-Gel Sci. Technol.*, 2010, vol. 21, pp. 39–48.
45. Metikoš-Huković, M., Tkalčec, E., Kwokal, A., and Piljac, J., *Surf. Coat. Technol.*, 2003, vol. 165, no. 1, pp. 40–50.
46. Mirhosseini, N., Crouse, P.L., Schmidt, M.J.J., Li, L., et al., *Appl. Surf. Sci.*, 2007, vol. 253, no. 19, pp. 7738–7743.